IJCRT.ORG ISSN : 2320-2882

INTERNATIONAL JOURNAL OF CREATIVE RESEARCH THOUGHTS (IJCRT)

An International Open Access, Peer-reviewed, Refereed Journal

Comparison Of The Aerodynamic Characteristics Of A Re-Entry Vehicle With Two Different Double Delta Wing Configurations: A Numerical Study.

Debivarati Sarangi*, Pravajyoti Patra, Dr. Subhas Chandra Rana***, Dr. T. Murugan******

Research scholar* Department of Mechanical Engineering
NIT Durgapur, India

Assistant Professor**
Department of Mechanical Engineering
CV Raman Global University

Assistant Professor* Department of Mechanical Engineering**
NIT Durgapur, India

Senior Scientist****
Thermal Science Division
Central Mechanical Engineering Research Institute, Durgapur

Abstract

Re-entry vehicles with double delta wing configuration are becoming an important topic of study in recent times due to the interest of many countries in space endeavor. Many studies are being performed with double-delta wings having different strake and wing swept angles with modification in wing profiles. In the present study, a re-entry vehicle having a reflex aerofoil at the bottom and two different NACA symmetrical aerofoils at the top surface of the wing are examined in detail by solving the Euler's equations using explicit first order upwind scheme for a free stream Mach number two. The angle attack of the vehicle is varied from 10^0 to 50^0 in steps of 5. The coefficients of pressure, Mach number, density gradient at different span wise locations, and the overall lift and drag coefficients are used for characterizing the vehicles wing platform for the descent phase at an altitude of 60000ft. It has been observed that the variation of lift coefficient in both NACA0012 and NACA0020 is negligible up to 35^0 and it has increasedto 18.48% in NACA0020 compared NACA0012 as the angle of attack increases. However, the NACA0020 aerofoil has shown an increase in drag coefficient from 2.57% to 18.43% compared to NACA0012 depending on the angle of attack. It suggests that NACA0020 could be used if more storage space is desired inside the wing as the variation in drag coefficient is within the limit.

Keywords: NACA0020**,** NACA0012**,** Euler's equation, Mach number, Density gradient, Force coefficients

I. INTRODUCTION

Recently, many developing countries such as India, China, Pakistan, etc. are focusing on ballistic and re-entry vehicles development to improve their global competence in space science and technology similar to United States of America, Russia, Great Britain, Germany, and Japan. These countries are carrying out in depth research on high altitude vehicles to achieve higher aerodynamic performance to fulfil the need of higher speed, greater maneuverability and higher aerodynamic efficiency at all flow regimes starting from low subsonic to hypersonic Mach numbers (M) and different altitudes. The vehicles flies in lower altitude are designed using cambered aerofoils with high thickness (t) to chord (c) ratio (t/c)for getting maximum lift at subsonic speed as the lift is proportional to square of the velocity. However, the wing configuration is designed differently by minimizing the frontal area and t/c to overcome the effects of compressibility such as wave drag, sonic boom, shock-boundary layer interaction for obtaining superior performance at tremendous speeds. Delta wings are used in fighter aircrafts to minimize the drag and increasing the maneuverability at supersonic speeds and it has a very less lift coefficient (CL) compared to the cambered aerofoils. A double delta wing is preferred in all re-entry vehicle to make the vehicle more compact by reducing the span and improving the aerodynamic performance in all M regimes. It also has superior aerodynamic performance at higher angle of attacks and at low subsonic speed during landing compared to delta wing. Further, it also gives a high internal fuel volume even at a relative low thickness due to a large and thick root chord. Several studies have been conducted on double delta wing by varying the strake and wing sweep angles for different Reynolds (Re) and Mach numbers to examine the most appropriate strake and wing combination. Much of the above studies are devoted to examine the performance of the double delta wing at low speeds **[1-3]**.

The flow over a 76^0 slender wing and two $76^0/60^0$, $76^0/40^0$ double delta wings were examined using laser sheet based smoke flow visualization to develop accurate computational methods. The results obtained from numerical method using free vortex sheet method were compared with experimental results. They found that the flow pattern over the double delta wings consistsof a single-branched strake vortex and a double-branched wing vortex and proposed a vortex sheet method **[4]**. A numerical investigation was performed on a flat $80^0/45^0$ double delta wing to examine the aerodynamic performance using free vortex sheet method developed by Boeing aircraft company. He had modeled the free vortex sheet in three ways and compared the results with experiments. Two separate vortex systems, one on the inboard and the other on the outboard leading edges were considered in the first case. A single vortex system along the leading edge was assumed in the second case and a separated flow on the inboard leading edge with an attached flow on the outboard leading edge was deliberated in the third case. He observed that the model that employs two separate vortex systems predicts the aerodynamic characteristics best agreement with the experimental data **[5]**.

A computational study of three-dimensional vortical flow over a round-edged $80^0/60^0$ double-delta wing was performed by solving Navier Stokes equations using an implicit upwind relaxation finite-difference scheme for Re=1.3*106. The vortex formation and interaction of strake and wing vortices were well captured and the computed static pressure distributions and lift coefficients were in good agreement with the experiments up to an angle of attack (α) of 25^0.The detailed structures of the vortical flow field was not predicted well with coarse grid though it had shown good agreement in lift coefficient and static pressure distributions **[6]**.

The effect of test section wall on the aerodynamic performance of $76^0/40^0$ double-delta wing was examined in a subsonic wind tunnel **[7]**. He had provided an overview of tunnel wall correction methods existing in the literature for wings with leading-edge vortex separation and corrected the surface-pressure data of a $76^0/40^0$ double delta wing using a correction method based on attached flow theory and CFD solution. The estimated wall corrections and the corrected pressure data compared reasonably well with data taken in a larger tunnel. The effects of strake plan form configurations of double-delta wings were examined through pressure measurements, flow visualization and PIV measurements **[8]**. He found that the strake modification could

greatly alter the vortex flow pattern around the delta wing and suggested that an actuator efficiently realizing the strake shape modification can be used as an effective tool for the active flow control of the vortex flow. He also found that 79^0 delta wing produced a more concentrated vortex system compared to $65^0/90^0$ and $72^0/84^0$ cropped delta wing. However, this vortex system diffused and broke down much faster as the flow proceeded to the downstream. The lift, drag, and pitching moment generated from a 65^0 delta and $65^0/40^0$ double-delta wings were examined using wind tunnel experiments and numerical simulations. The simulated results showed good agreementwith the experiments and theoretical calculations **[9]**.

The effect of Reynold's number on free stream vortices was examined. He found that the strake and wing vortex trajectories tend to move outboard closer to the model surface and the vortex breakdown location moves upstream as Re increases. The effect of fillet shape on 76^0 /40^0 double delta wing was studied for M varying from 0.18 to 0.7 **[10]**. A numerical comparative study of NACA 6409 and NACA 4412 aerofoil was performed using viscous laminar model. They measured the drag coefficient, lift coefficient and overall pressure distributions at 0^0 and 5^0 angle of attacks and for velocity 1m/s. They found that for all angle of attacks NACA 4412 aerofoil provides more practical result **[11]**. Studies were also performed inthe literature to observe the highly nonlinear effect of shock wave, shock-vortex interaction and other complex phenomenon caused due to the flow that takes place over the double delta wing in the supersonic regime **[12]**. He found that shock waves produced a considerable temperature rise by real gas effects to cause severe heating problems at high Mach numbers. The interaction of shock waves produced complex wave patterns containing slip-lines and associated shear layers whose impingement on a nearby surface caused detrimental pressure and heat transfer. The impact of a shockwave on the boundary layer was the origin of strong viscous interactions and it remained a limiting factor in the design of transonic wings, supersonic air intakes, propulsive nozzles and compressor cascades. The vortical flow field over a 65^0 sweep, sharp leading edge, non-cambered delta wing was investigated using surface reflective visualization system. It was found that bothsymmetric and asymmetric vortex break down were noticed over the wing and they were influenced by the shock wave **[13]**. A computational study to examine the interaction of a planar shock wave with a sphere **[14]**.

They observed the vibration caused by the shockwave over a hemisphere at supersonic speed. The numerical simulations of a compound delta wing was performed at various M ranging from 0.3 to 2.0 and alpha ranging from 0 ◦ to 15 ◦. Steady-state computations were performed using RANS based (SA) turbulence model. They observed that flow near to the delta wing surface beneath the primary vortex becomes fully supersonic and a shock wave appeared whenthe M reaches to 0.85. They also found that the primary vortex prevented the evolution of the inner separation and the subsequent formation of secondary vortex due to its stronger vorticity **[15]**. A vortex flow characteristic over a sharp edged delta wing was studied **[1]**.

He has considered a three dimensional, compressible Reynolds-averaged Navier-Stokes equation to understand the effects of the angle of yaw, angle of attack, and free stream velocity on the development and interaction of vortices and the relationship between suction pressure distributions and vortex flow characteristics. He found that with an increase in the angle of yaw, the symmetry of the pair of leading edge vortices was broken and the vortex strength was decreased on both windward and leeward sides and also an increase in the free stream velocity resulted in stronger leading edge vortices with an outboard movement.

There were two practices of understanding flow behavior prior to 1960, one is analytical approach and another is the experimental approach. The analytical study is perfumed by linearizing the governing equations and it is quite straight forward. But the experimental study of aerodynamics is quite expensive and cumbersome. Computational fluid dynamics in the 1960s brought a frugal and harmless approach to study and analyze the flow physics of these re-entry vehicles using Ansys-Fluent, CFX and CFD post processing. It offers both quantitative and qualitative results such as visualization of flow regimes surrounding a subjected model, redesigning of the model, with quick reanalysis, fast and effective approach to researching and solving problems related to fluid dynamics. Therefore an Eulerian computational model is adopted for both the NACA profiles to investigate the flow physics at various angle of attacks and Mach two. Recent technological

advancement in defense systems emphasizes the need for high-lift and low-drag vehicles in a broad range of angles of attack, specifically the advanced superior maneuverable fighter aircrafts and missiles **[15]**. Therefore, in this paper, Ansys Fluent based numerical study is performed to analyze the aerodynamic characteristics of re-entry vehicle. In this paper, a re-entry vehicle having double delta wing with a strake and wing angles of 80 ◦ and 45 ◦ is examined by varying the angle of attack from 10 ◦ to 50 ◦ and the thickness of the symmetrical wing. Two different thicknesses to chord ratio of four digit NACA aerofoil namely, 12 and 20% are considered. The free stream Mach number is 2.

II. CONCEPTUAL RE-ENTRY VEHICLE'S CONFIGURATIONS

The 3-D model of the conceptual re-entry vehicles developed using Solidworks is shown in **Fig.1**. Both the profiles have double delta wing configuration with strake and wing swept angle of 80^0 and 45^0 respectively. The aspect ratio of the wing platform is 2.16. The upper surfaces of the wings and strakes have the NACA 0020 aerofoil profile and NACA 0012 profile, and for both case reflex aerofoil profile is considered at the bottom. The reflex profile is chosen for the bottom surface to minimize the wave drag. Both of the re-entry vehicles have a maximum length of 2220 mm with a total span length of 2600 mm. The wings have a root and tip chord length of 1270 mm and 330 mm respectively. The strake and wing were combined through an arc having a radius of curvature of 1000 mm. The re-entry vehicles were scaled down to 1:25 to minimize the computation time. The blockage ratio (Fig.2) of the virtual wind tunnels were 2.73% and the height of the domains were chosen in such a way that the reflected shock waves from the wall do not interact with the model. The simulations were performed for α varying from 10^0 to 50^0 in steps of 5^0. As the focus of the present study is to examine the characteristics of double-delta wing, fins were not considered in the simulations. The flow over the top surfaces of both the profiles were emphasized as variations in coefficients (CL, CD) with α which depend on the nature of flow over the top portion.

III. DETAILS OF NUMERICAL SIMULATIONS AND REFERENCE SCENARIO

Figure.2 shows the 3-D computational domain and a sectional view of the meshing done over the vehicle at the mid-span. The 3D fluid domains were created around the vehicle as an enclosure shown in **Fig.2a** using Ansys Fluent. The models were placed at three times mean chord length from the inlet for both cases and the fluid outlet was kept at ten times the mean chord from the rear end of the vehicle. This greater distance was chosen to observe the far field characteristics of the vortical flow. The top, bottom and side walls were kept at a length of 2.5 times the mean chord. The computational domain was discretized with a hexagonal mesh as shown in Fig. 2b using Ansys fluent software. The simulations were performed for both the profiles using inviscid models for α varying from 10 ◦ to 50 ◦ in steps of 5 ◦. A total of eighteen (18) models were developed, and 18 different cases were simulated in the present computational study. The simulations were performed for a free stream Mach number (M) of 2, and the altitude of the vehicle was 60000 ft.

The atmospheric conditions at this altitude were determined using the NASA online calculator. The pressure, temperature, and free stream velocities were 7171.64 Pa, 216 K, and 296 m/s respectively. The mass flow inlet boundary condition was applied at the entrance of the computational domain, and the pressure far-field outlet condition was taken at the exit. No-slip boundary condition was considered at the surface of the vehicle and all virtual wind tunnel boundaries. A steady-state density based solver with Advective Upstream Splitting Method (AUSM) scheme is used for characterizing the flow past the re-entry vehicle for NACA0012 and NACA0020 profiles. The drag and lift coefficients were monitored, and the convergence criteria was taken as 10^{-6} for flow variables.

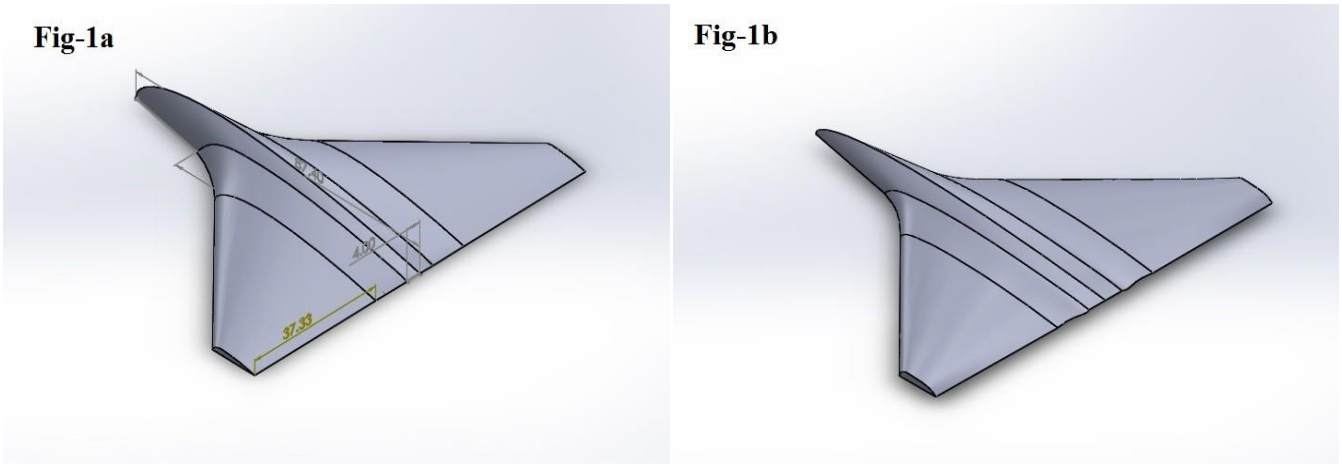

Figure 1: Isometric view of Re-entry vehicle (a): NACA0020 profile. (b): NACA0012 profile.

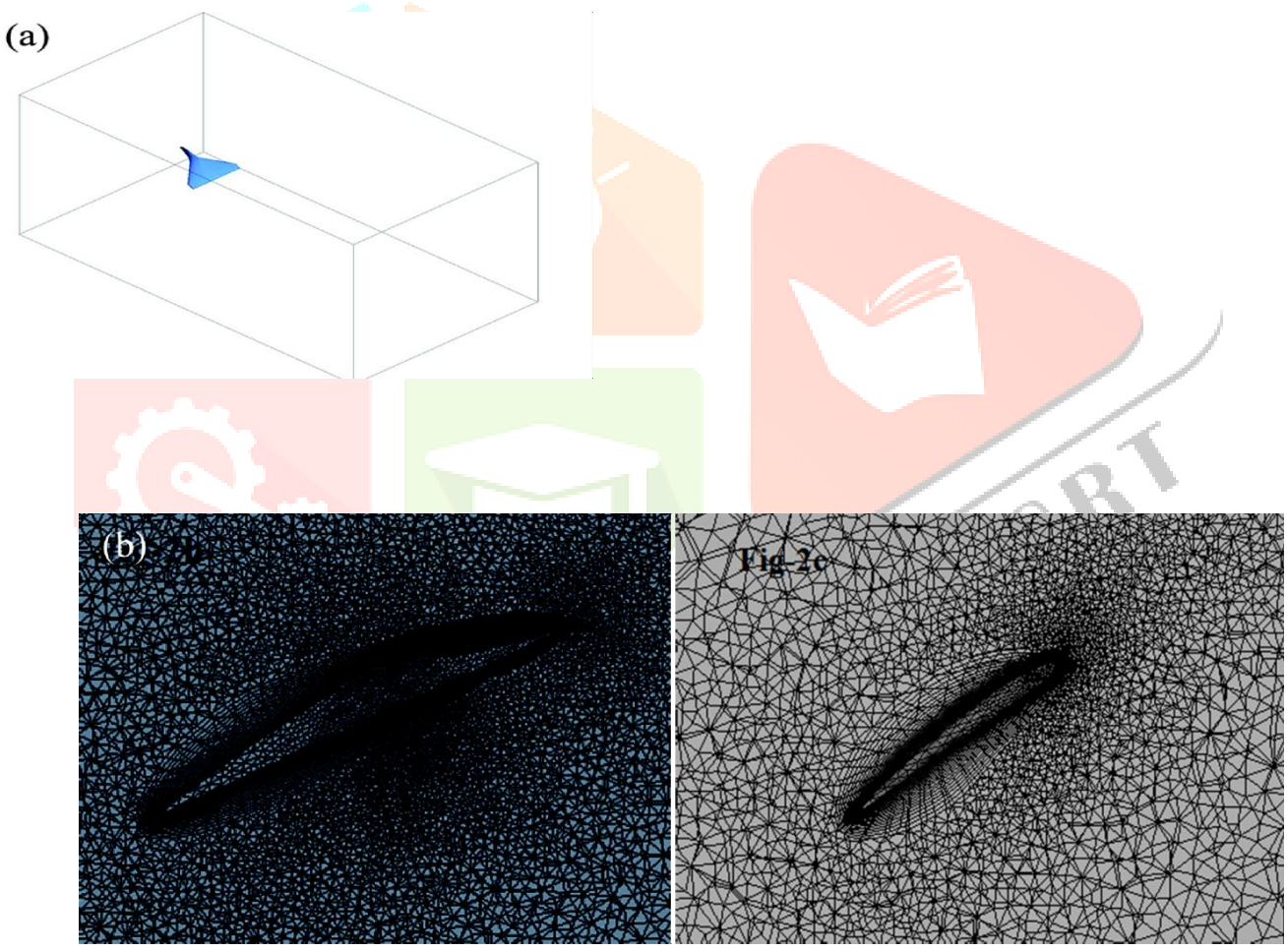

Figure 2: (a): Computational domain of NACA0020. Sectional view of Meshing of re-entry vehicle (b): NACA0020 profile. (c): NACA0012 profile.

IV. ANALYSIS OF NUMERICAL RESULTS AND DISCUSSIONS

A. GRID DEPENDENCY STUDY

Grid dependency studies are essential for any numerical simulation to obtain a unique solution irrespective of the fineness of the grids. Here, the flow over the two conceptual re-entry vehicles is studied using inviscid model. Two grids having the number of elements 3.6 and 0.3 million respectively. **Figure.3** shows the variation of C_L and C_D with α varying from 10^0 to

50^0. For NACA0012 profile it is observed that up to 35^0 the variation of lift coefficient is less than 2% but beyond this variation of C_L is increasing. For all angle of attacks variation of results is less than 3.5% except at 50^0. Though 50^0 shows maximum variation i.e., 7.1% but our objective is to analyze the effect up to stall angle. Therefore it is not taken into consideration. And also for the NACA0012 profile, it is observed that the finer grid shows the optimum angle of attack at 35^0 but the coarse grid shows the optimum angle of attack between 35^0 to 40^0. The variation of Cd value between the coarse grid and fine grid for the NACA0012 profile is less than 1%. The variation of both C_D and C_L value between coarse grid and fine grid for NACA0020 profile is also achieved less than 1%. As the finer grid showed realistic gradual variations in C_L and C_D with α compared to the coarser grid, all simulations are performed using finer grid.

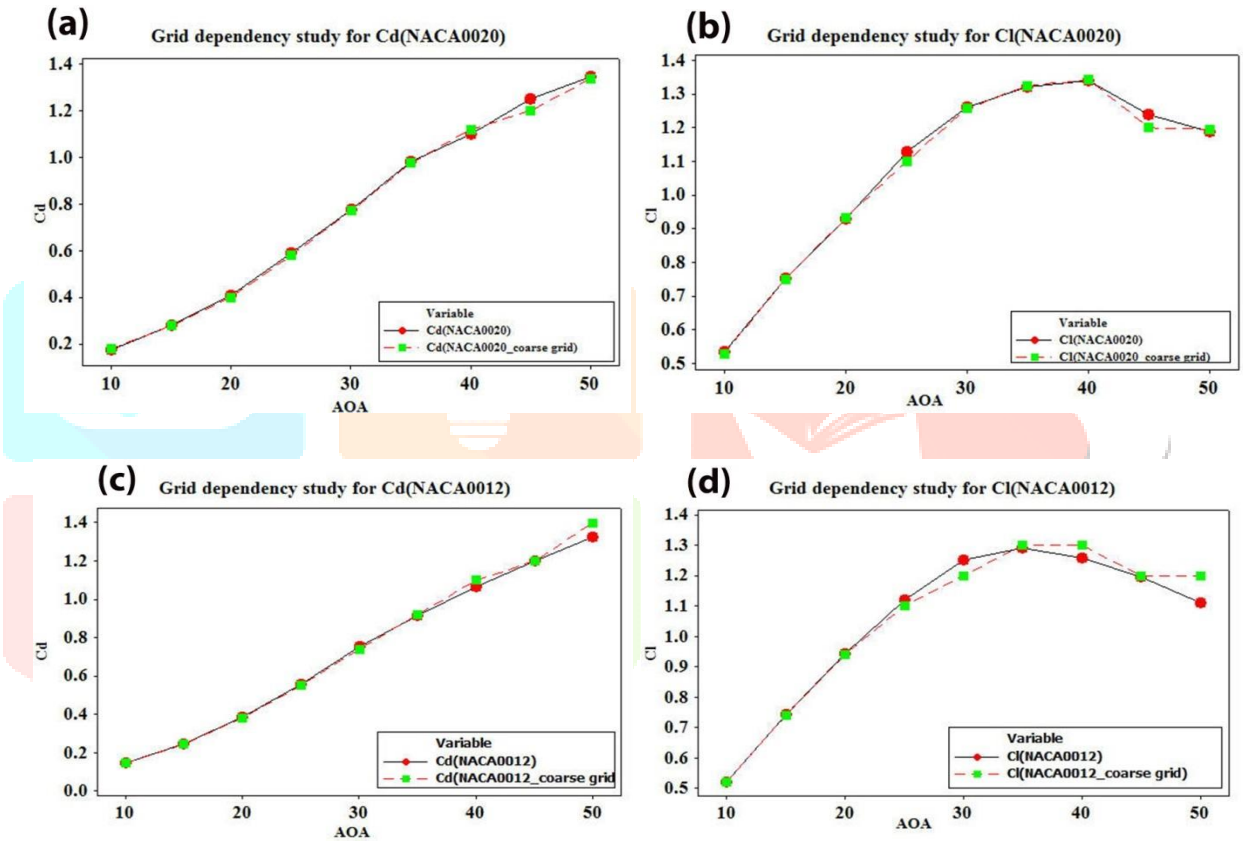

Figure 3 Grid dependency study for NACA0020 and NACA0012 profile (a): C_D for NACA0020 (b): C_L for NACA0020 (c) C_D for NACA0012 (d): C_L for NACA0012

The effect of angle of attack on lift coefficient, drag coefficient, shock strength and shock pattern of an $80^0/45^0$ reentry vehicle of double delta wing configuration with NACA0012 profile and NACA0020 profile at Mach number two is simulated. The inviscid model is used in the simulation as supersonic flows are generally treated as inviscid. Since the study involves supersonic flow simulation density based solver is used to incorporate the effect of compressibility in the computational model. Monitored value from the force convergence monitor was used to calculate drag coefficient, lift coefficient and the result of lift and drag coefficients obtained at the different angle of attacks for NACA0012 and NACA0020 profiles are compared and plotted to find out the best profile. Strake and wing vortices and flow transition is shown in the vorticity plots. Density gradient contours are plotted for both NACA0012 and NACA0020 profile using CFD Post processing to capture the shock wave pattern and to find out the shock strength. The shock wave contours are plotted at mid-span, 20% span, 40% span, 80% span. Pressure coefficient values are plotted at 10%, 20%, 40%, 60%, and 80% of chord length to find out the zone of separated flow and the zone with maximum and minimum lift coefficients and similarly the

Mach contours and corresponding sectional Mach plots are shown to give a clearer picture of the flow behavior.

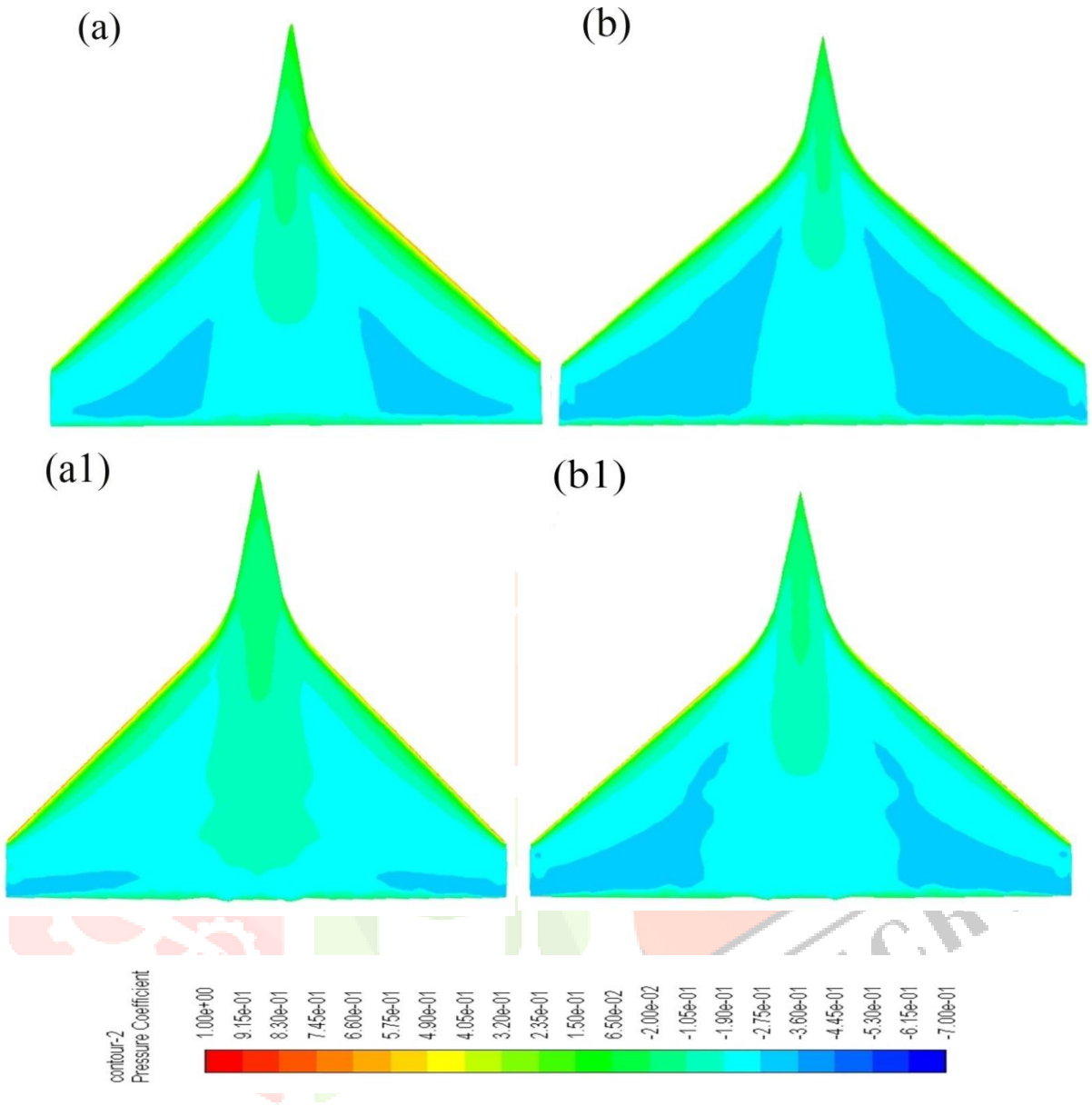
(a)
(b)
(a1)
(b1)
contour-2
Pressure Coefficient
1.00e+00
9.15e-01
8.30e-01
7.45e-01
6.60e-01
5.75e-01
4.90e-01
4.05e-01
3.20e-01
2.35e-01
1.50e-01
6.50e-02
-2.00e-02
-1.05e-01
-1.90e-01
-2.75e-01
-3.60e-01
-4.45e-01
-5.30e-01
-6.15e-01
-7.00e-01

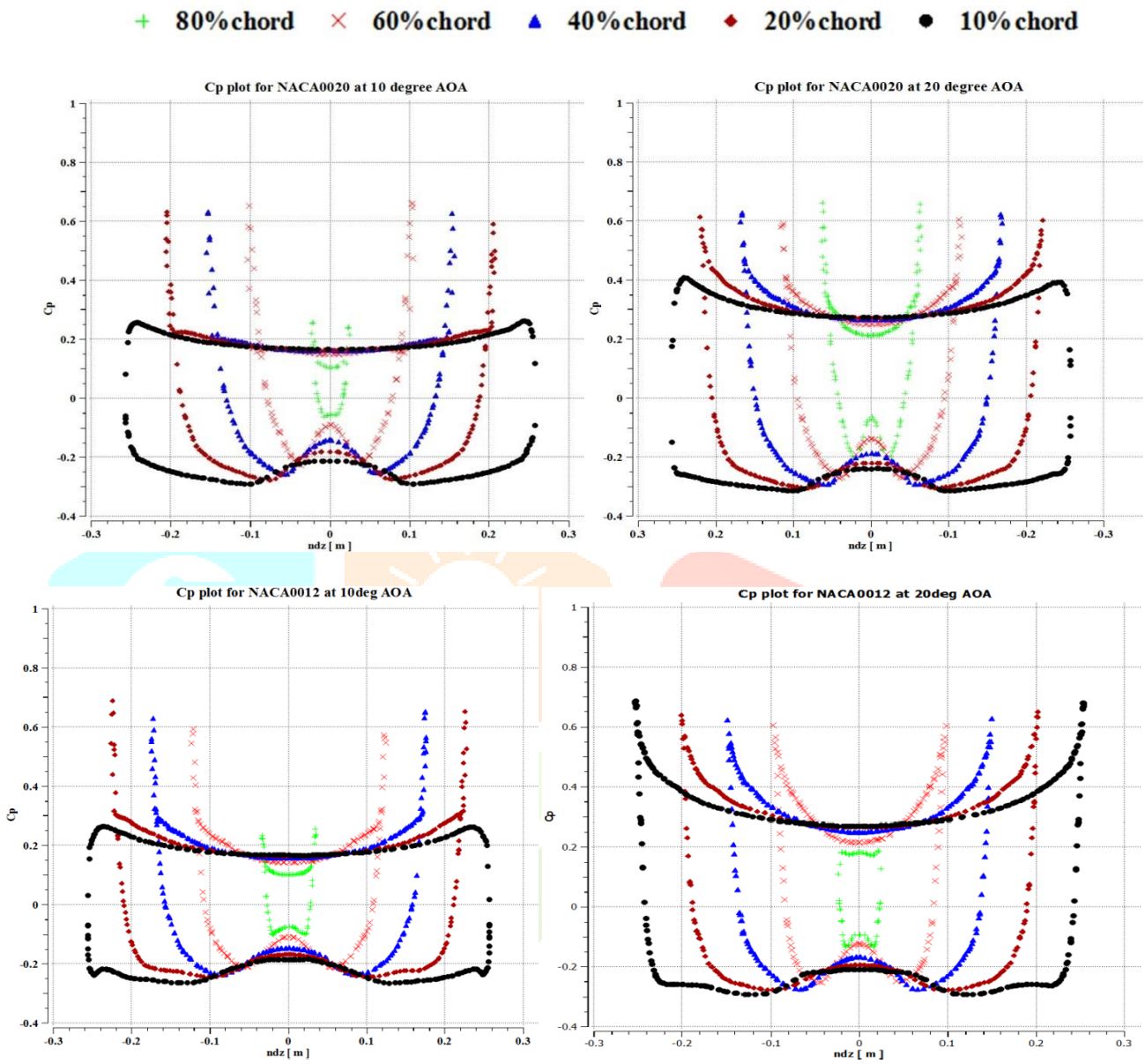

Figure 4 Pressure coefficient contour plots and corresponding sectional plots (*a*): Cp for NACA0020 profileat $\alpha=10^0$(*b*): Cp for NACA0020 profile at $\alpha=20^0$. (*a*1): Cp for NACA0012 profile at $\alpha=10^0$ (*b*1): Cp for NACA0012 profile at $\alpha=20^0$.

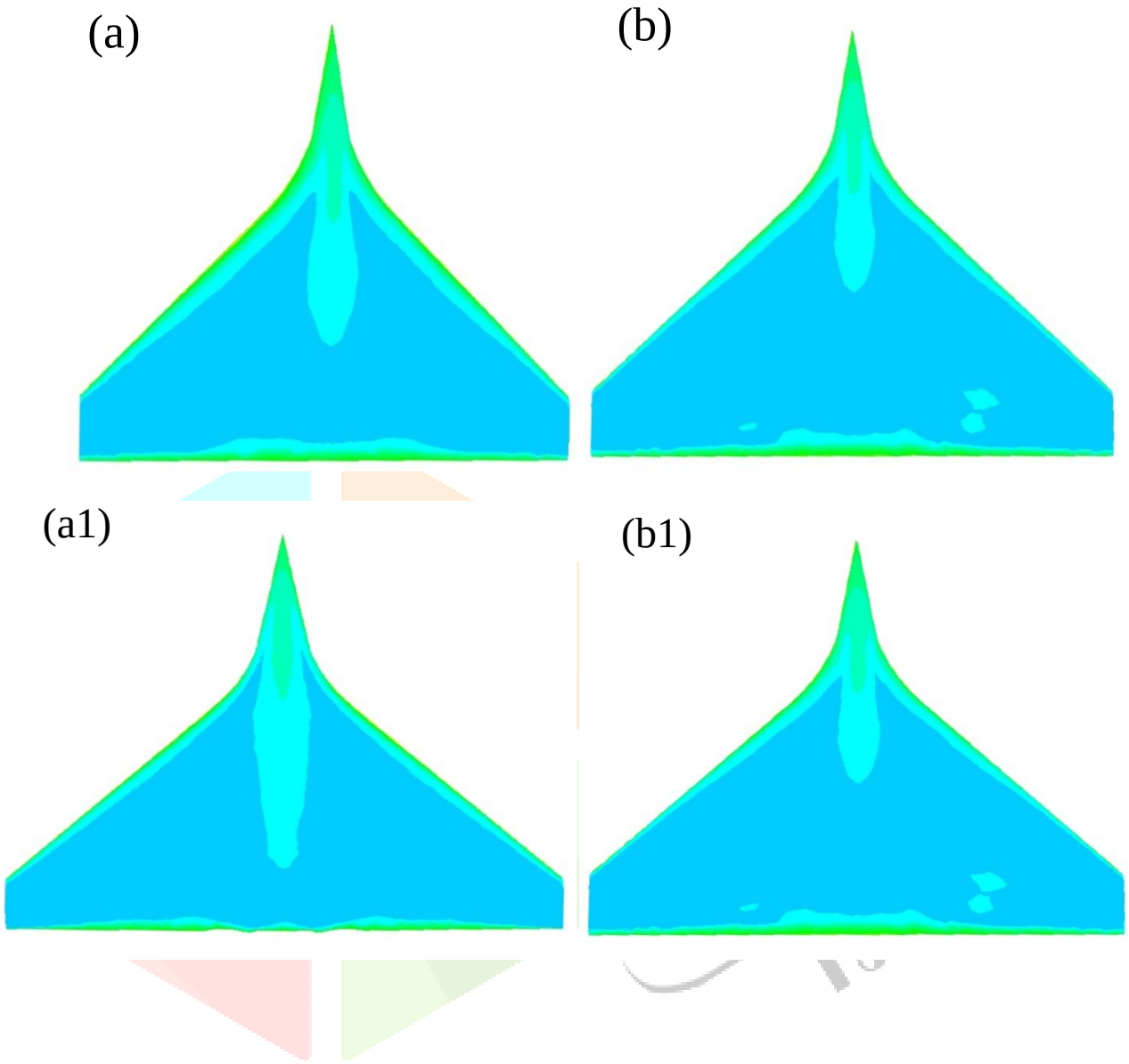
(a)
(b)
(a1)
(b1)

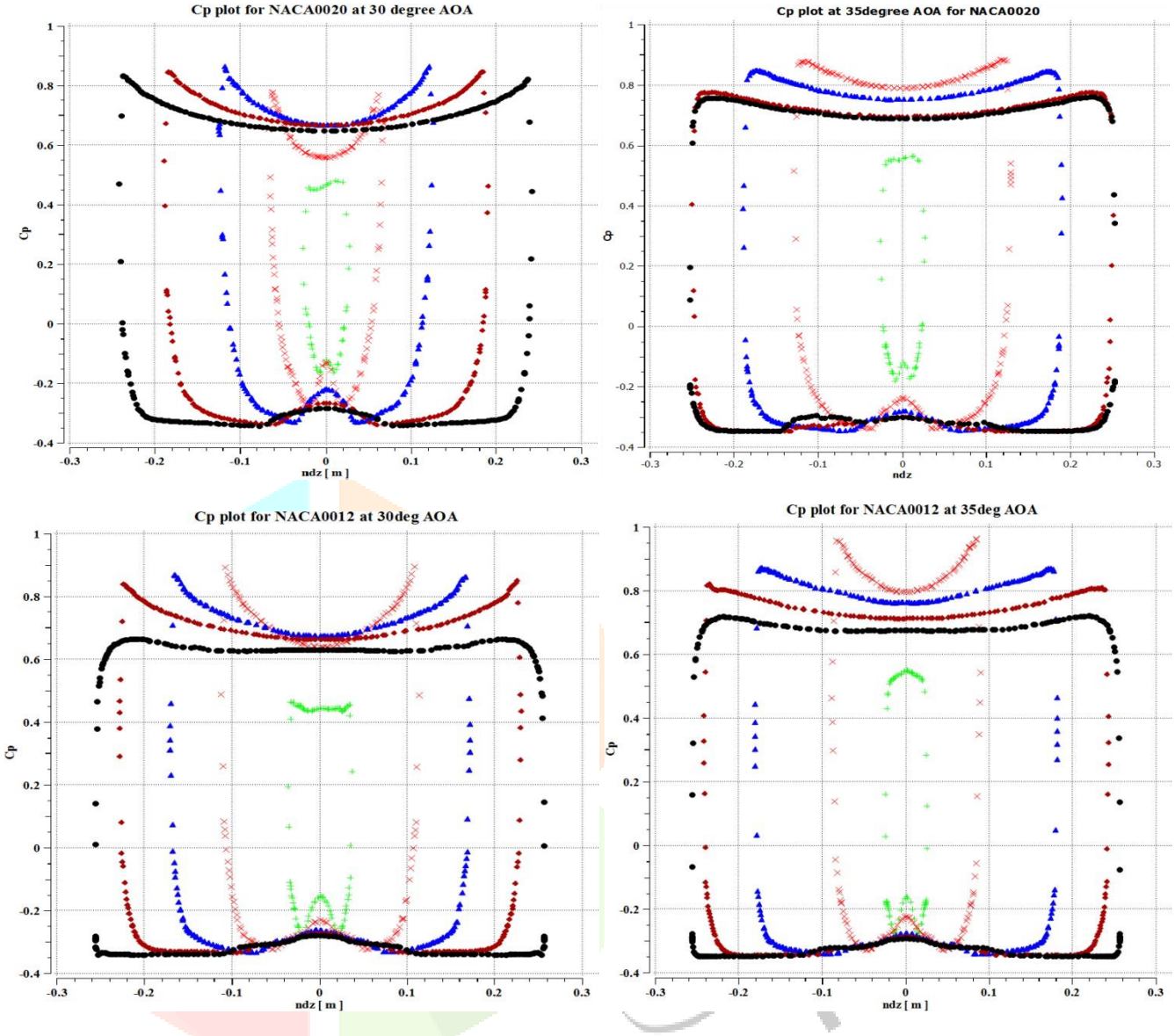

Figure 5 Pressure coefficient contour plots and corresponding sectional plots (*a*): Cp for NACA0020 profile at $\alpha=30^0$ (*b*): Cp for NACA0020 profile at $\alpha=35^0$. (*a*1): Cp for NACA0012 profile at $\alpha=30^0$. (*b*1): Cp for NACA0012 profile at $\alpha=35^0$.

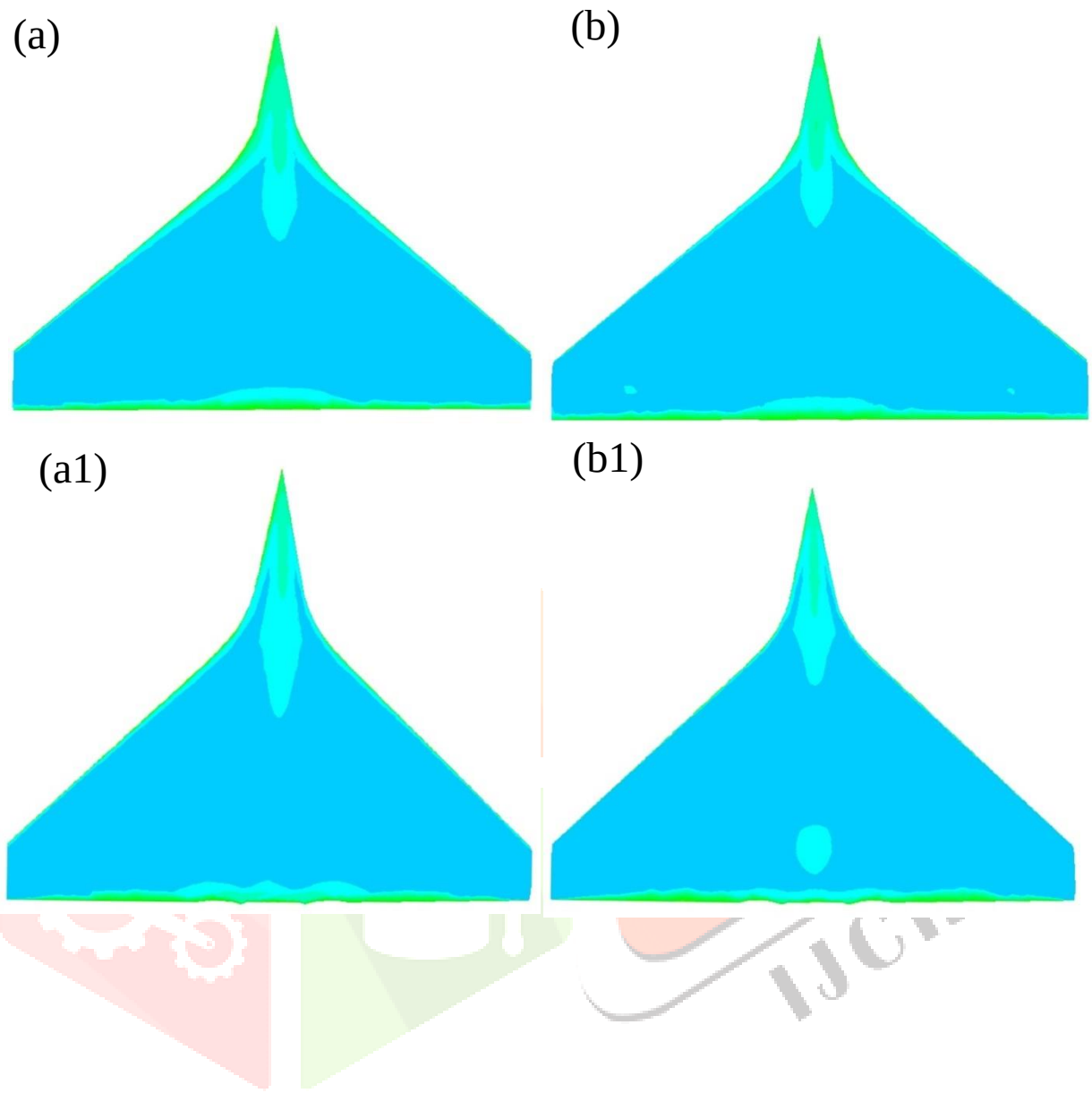
(a)
(b)
(a1)
(b1)

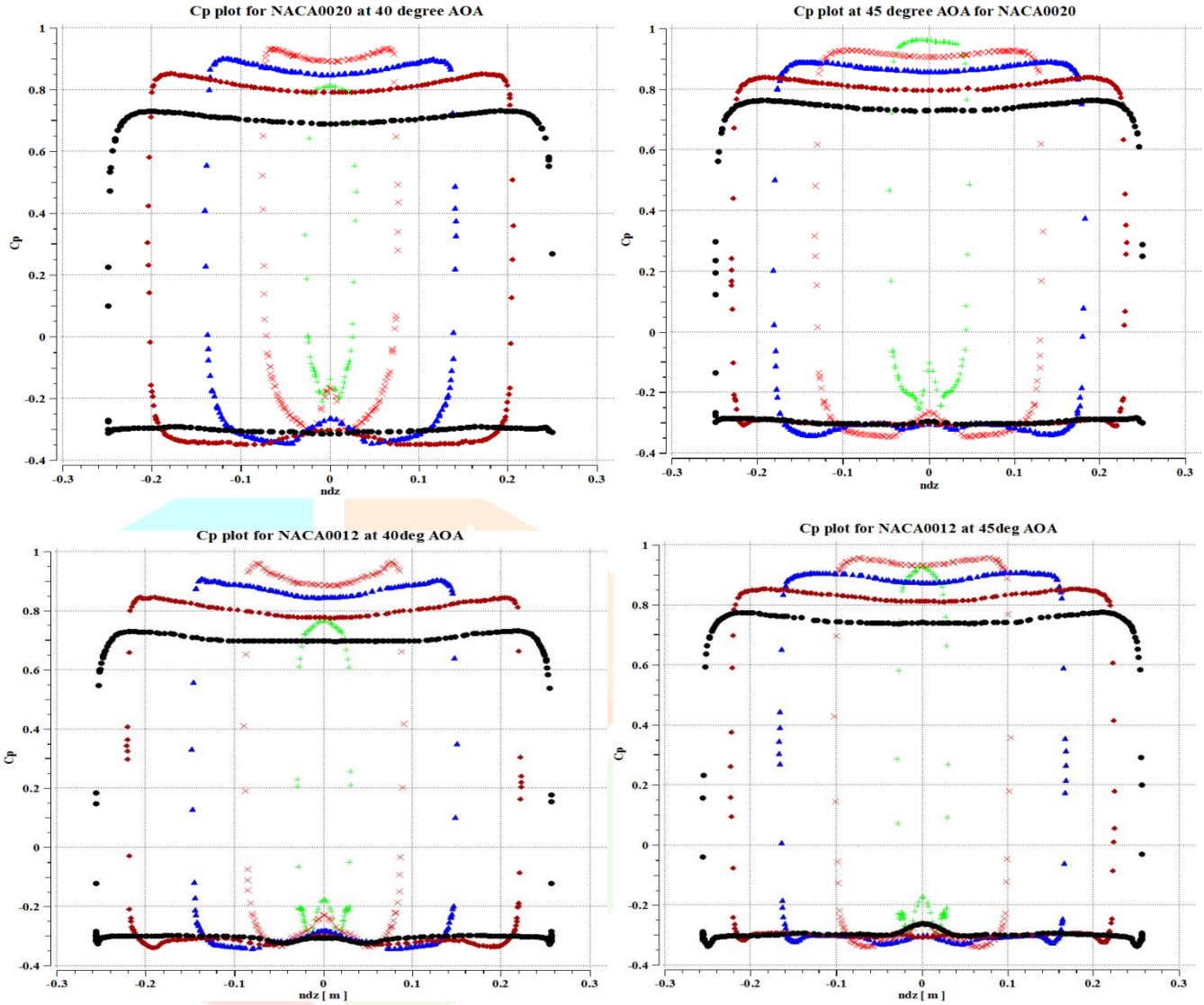

Figure 6 Pressure coefficient contour plots and corresponding sectional plots (*a*): Cp for NACA0020 profile at α=40^0 (*b*): Cp for NACA0020 profile at α=45^0. (*a*1): Cp for NACA0012 profile at α=40^0. (*b*1): Cp for NACA0012 profile at α=45^0.

B. COMPARATIVE ANALYSIS OF PRESSURE COEFFICIENT

Pressure coefficient contours for α 10^0, 20^0, 30^0, 35^0, 40^0 and 45^0 are plotted in **Fig.4, Figure.5 and Figure.6** for NACA0020 profile and NACA0012 profile to show the measure changes with respect to α and relative thickness. The pressure coefficient is a dimensionless number which describes the relative pressures throughout a flow field and it is used to calculate the sectional lift and drag coefficient value. From the pressure coefficient contour plots for α= 10^0 and 20^0,the suction surface of the vehicle with NACA0020 profile shows more negative Cp value compared to NACA0012 profile. The variation in pressure coefficient over the top and bottom surface of the re-entry vehicle at 10%, 20%, 40%, 60% (wing) and 80% (strake) of the chord length from the trailing edge are shown below the contour plots. For α=10^0 and 20^0 the peak observed near to mid-span (ndz=0) for both profile shows the presence of vortices over the wing and strake region. From the sectional plot more concentrated vorticity is observed for NACA0012 profile compared to NACA0012 profile. Thus higher C_L is expected for NACA0020 at α=10^0 and 20^0. For α=30^0 the strength of vorticity is found to increase over the strake region and higher peak is observed for NACA0012 profile. But the strength of wing vortices is found to decrease for NACA0012 profile. The flattening of Cp curve shows the initiation of the breakdown of vortex core region for NACA0012. Similar trend is observed for NACA0012 profile at α=35^0. But for NACA0020 profile the flattening of Cp curve initiates at α=35^0. This analysis predicts earlier stalling for NACA0012 compared to NACA0020. At α=40^0 and 45^0 the strake vortex is still intact for both the profile. At 60% and 40% of chord from the trailing edge vorticity is observed for NACA0020 where as it is found to be broken for NACA0012 (α=40^0). And at 20% and 10% of chord from the trailing edge vortex break down is observed for both the profiles. The variation of pressure coefficient has significant role in the variation of Mach number, vortex structure and other flow parameters. The flow behavior is more clearly described by the Mach contour and corresponding chord wise Mach number plots.

C. COMPARATIVE ANALYSIS OF MACH NUMBER

Mach number contours plotted for α varying from 10^0 to 45^0 are shown in **Fig.7, Figure.8, Figure.9** for NACA0020 profile and NACA0012 profile. From the Mach contours, for both the profiles, it is observed that near the mid -span Mach number is less than the Mach number near to the edges up to α=35^0. This shows a higher velocity at the edges compared to mid-span. Hence the lift coefficient value is found higher at the edges. Beyond this flow transition is observed which reduce the Mach number i.e., the velocity at the edges. Therefore a downward thrust is expected over the wing and strake region of re-entry vehicle. Because of this flow transition lift coefficient value is observed to decrease. Compared to NACA0012 profile, NACA0020 profile showed higher velocity i.e., higher Mach number over the wing. Also the less Mach zone over the strake region is more for NACA0012 compared to NACA0020. Thus higher CL value is expected for NACA0020 compared to NACA0012.

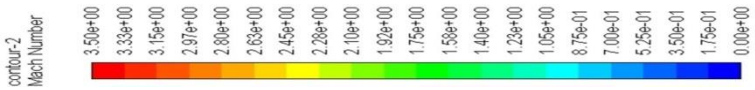

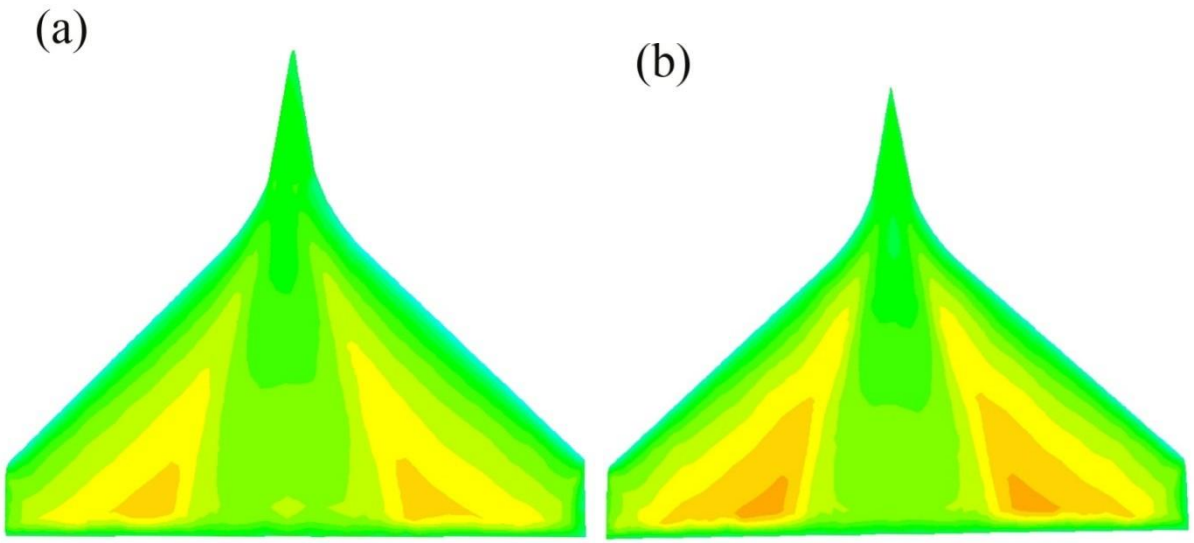
(a)
(b)

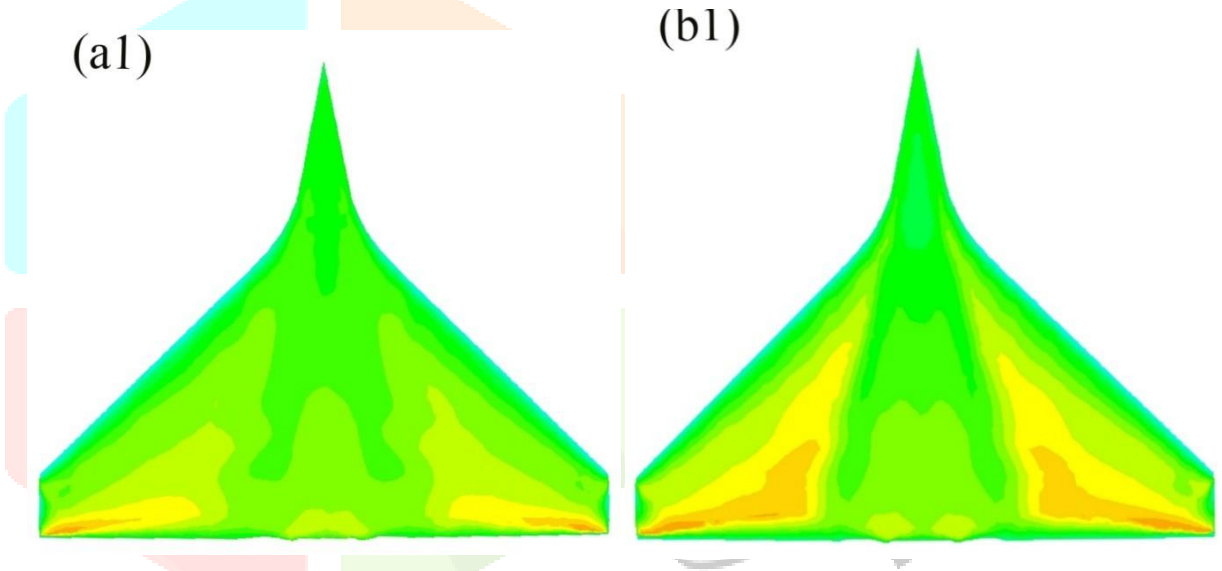
(a1)
(b1)

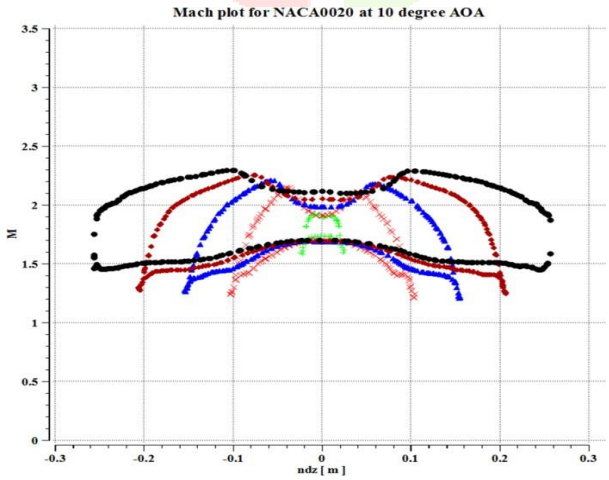
Mach plot for NACA0020 at 10 degree AOA
M
ndz [m]

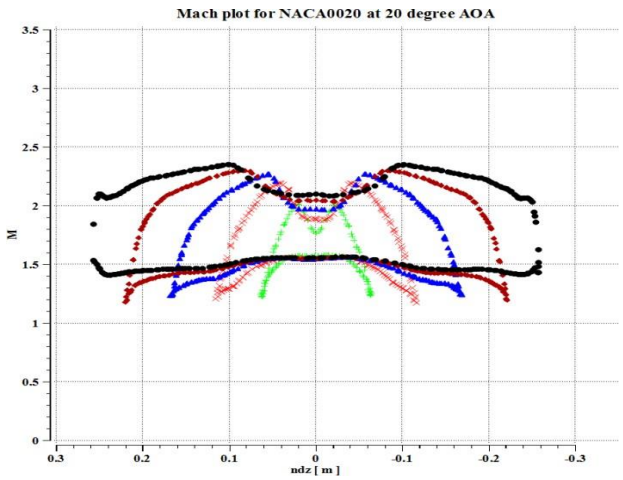
Mach plot for NACA0020 at 20 degree AOA
M
ndz [m]

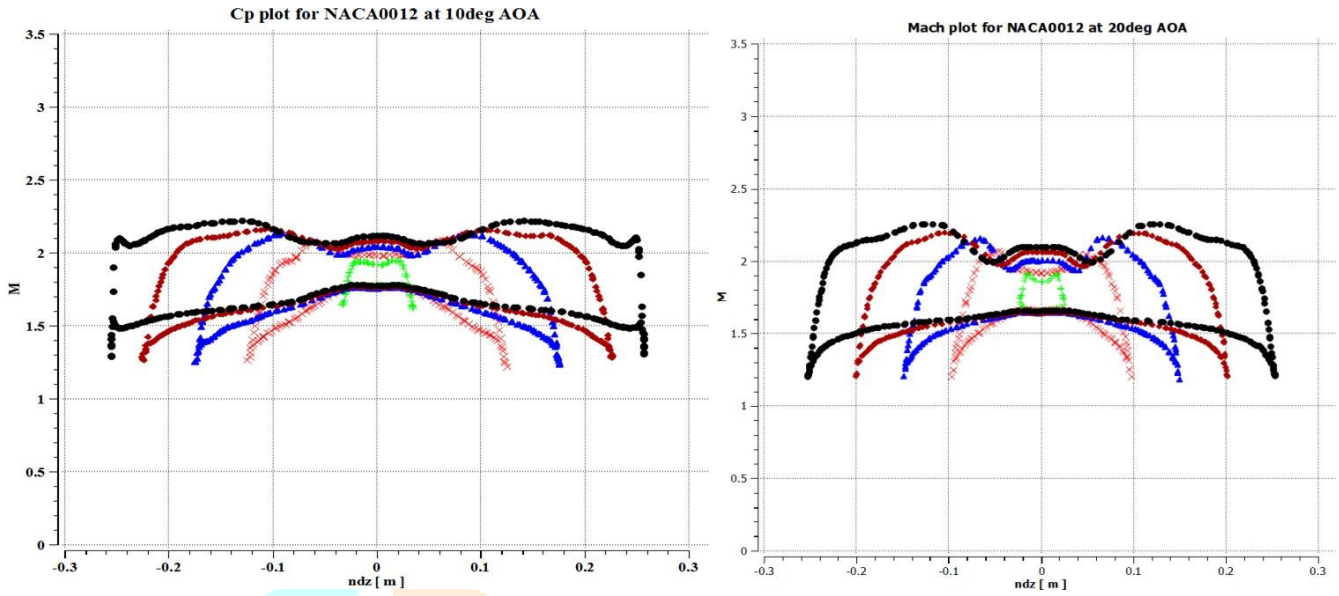

Figure 7 Mach contours and corresponding sectional plots (*a*): M for NACA0020 profile at $\alpha=10^0$. (*b*): M for NACA0020 profile at $\alpha=20^0$. (*a*1): M for NACA0012 profile at $\alpha=10^0$. (*b*1): M for NACA0012 profile at $\alpha=20^0$.

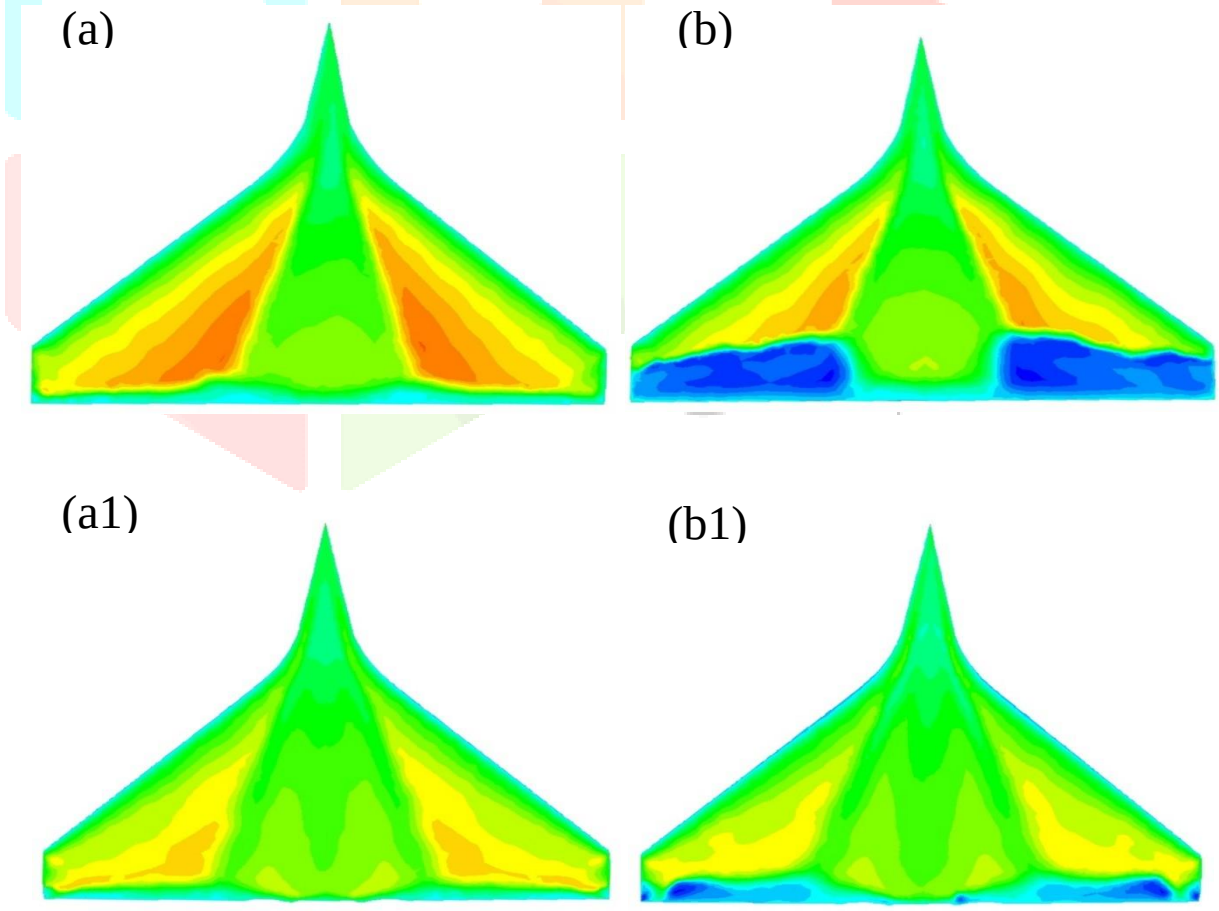

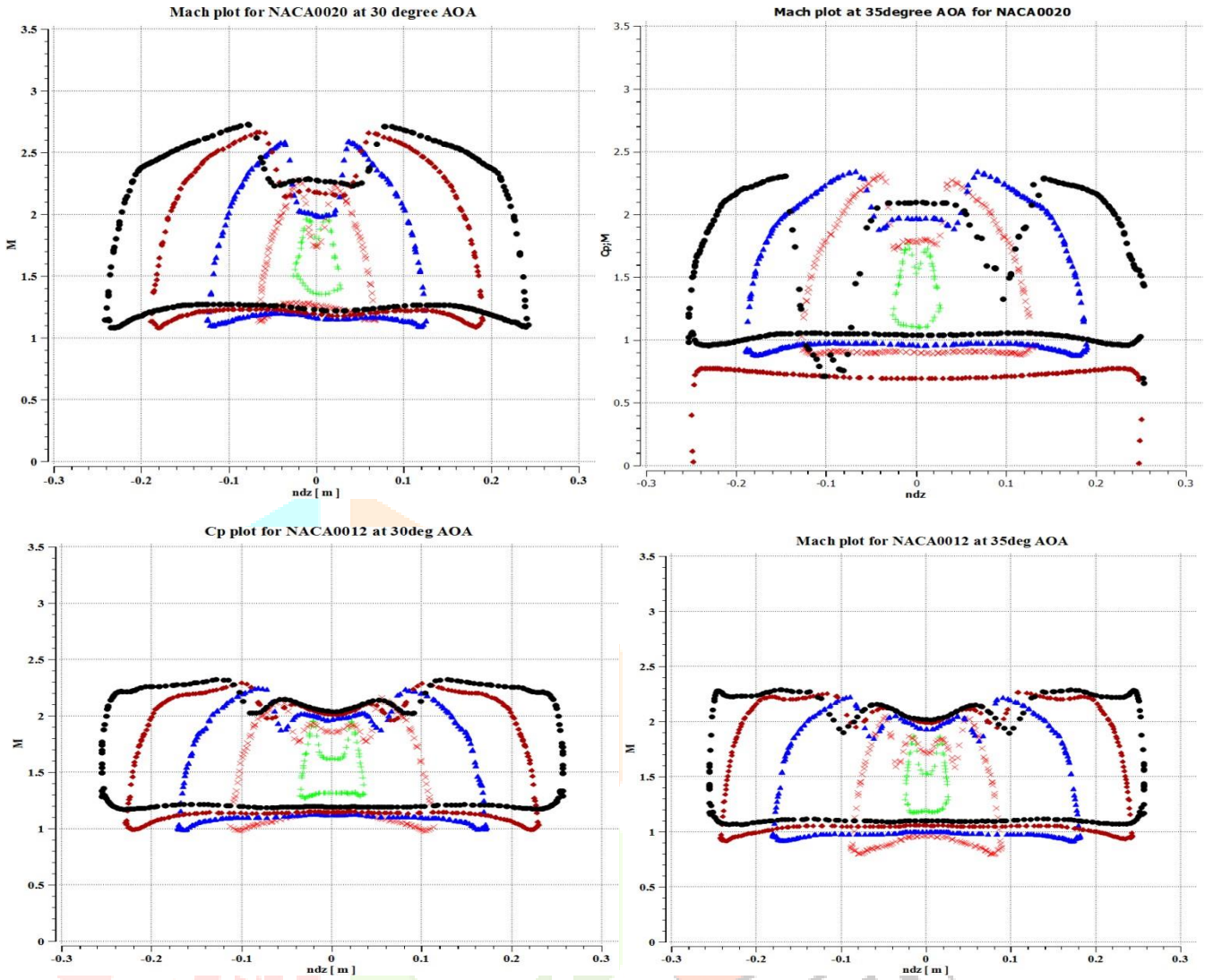

Figure 8 Mach contours and corresponding sectional plots (*a*): M for NACA0020 profile at α=30^0. (*b*): M for NACA0020 profile at α=35^0. (*a*1): M for NACA0012 profile at α=30^0. (*b*1): M for NACA0012 profile at α=35^0.

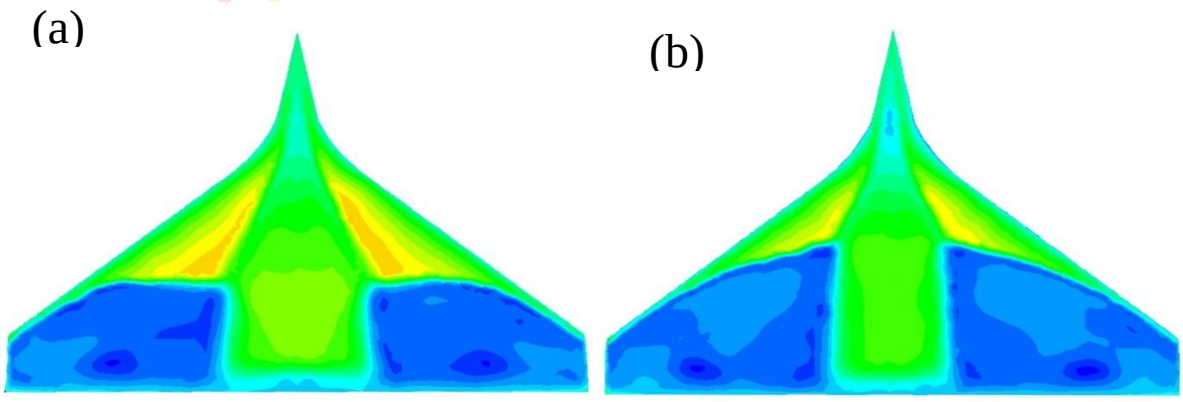

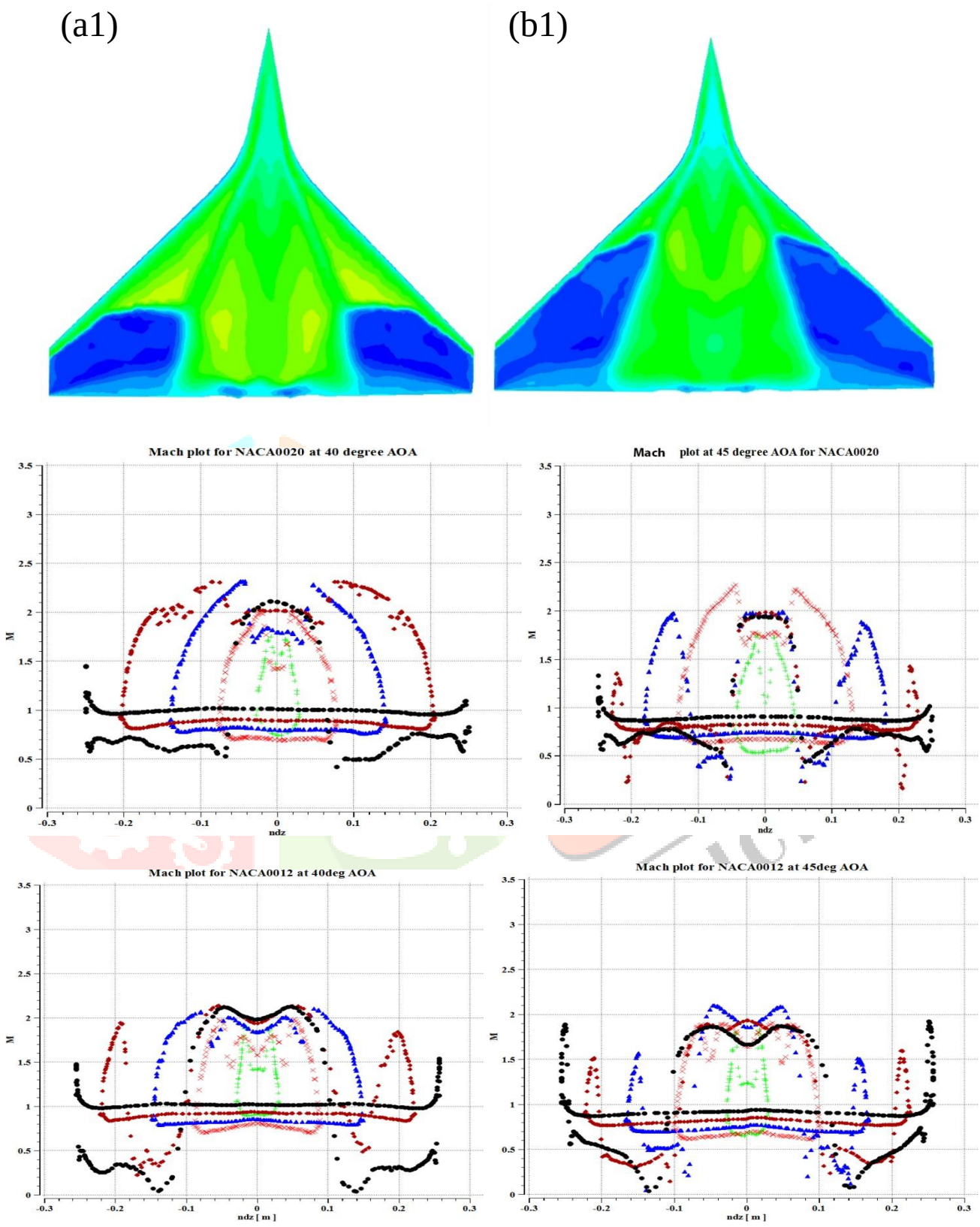

Figure 9 Mach contours and corresponding sectional plots (*a*): M for NACA0020 profile at $\alpha=40^0$. (*b*): M for NACA0020 profile at $\alpha=45^0$. (*a*1): M for NACA0012 profile at $\alpha=40^0$.(*b*1): M for NACA0012 profile model at $\alpha=45^0$.

D. COMPARATIVE ANALYSIS OF SHOCK STRUCTURE

Schlieren technology relies on the fact that light rays are bent whenever they encounter changes in density of a fluid and it is used to capture shock wave patterns. The same principle is applied in CFD Post-processing to capture shock waves and density gradient variable is used to plot shock wave pattern. Density gradient magnitude at mid-span, 20% span, 40% span and 80% span are shown in line plots in **Fig.10, Fig.11 and Fig.12** for both NACA0020 profile and NACA0012 profile. This shows that magnitude of shock strength is less at mid-span and 20% of span in comparison to 40% and 80% of span because of the detached shock formation at 40% and 80% span. It is also observed that the density gradient magnitude is higher for the NACA0012 profile compared to NACA0020 profile. This indicates the formation of a stronger shock for NACA0012 profile. The qualitative images are also plotted in CFD post-processing which shows the presence of shock wave at different portions of the span length as shown in **Fig.13**. Also this shock wave seems to interact with the vortex structure there by creating vortex breakdown as described in the consequent section.

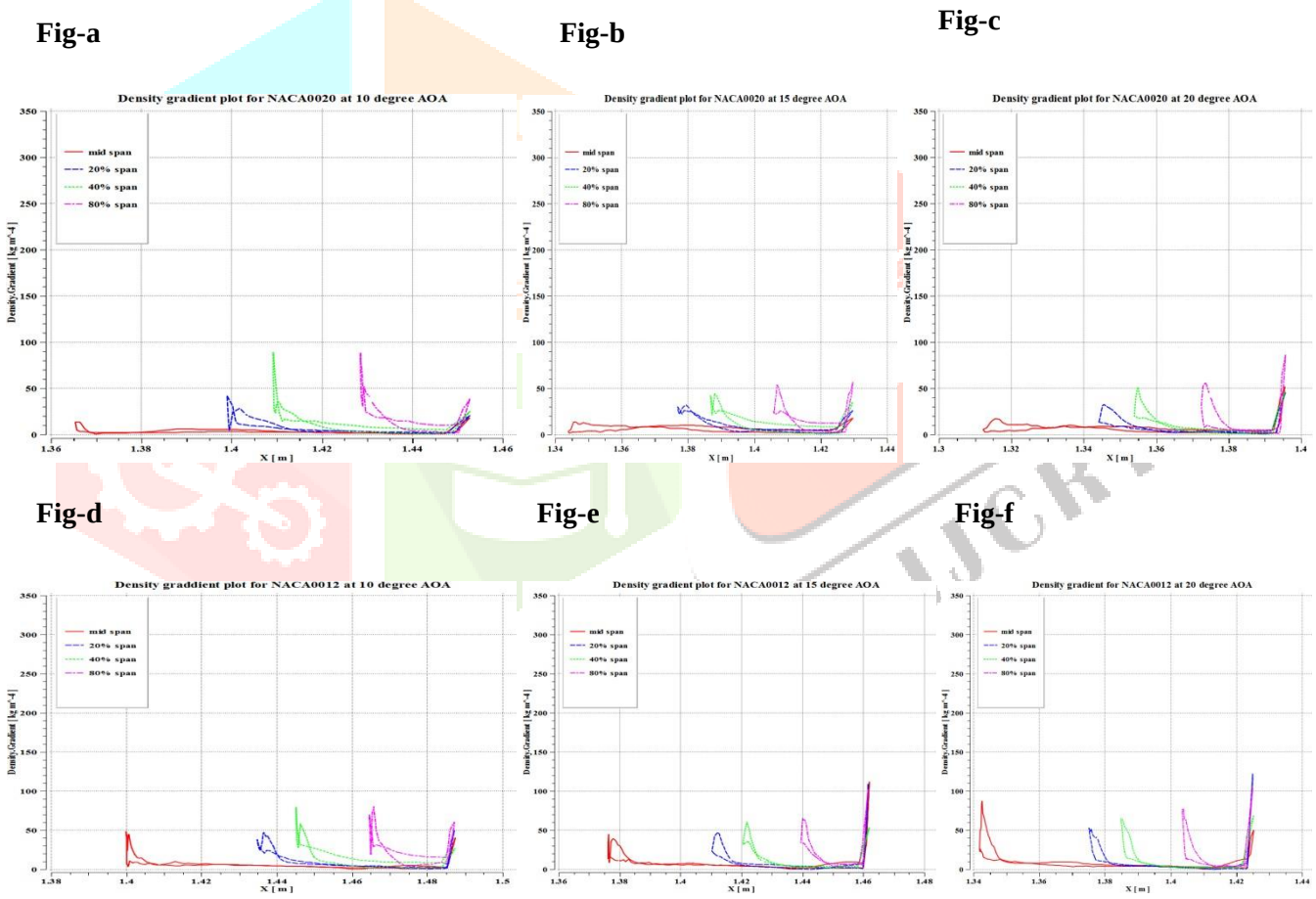

Figure 10 Density gradient span-wise plots (*a*): $\nabla \rho$ plot for NACA0020 profile at $\alpha=10^0$. (*b*): $\nabla \rho$ plot for NACA0020 profile at $\alpha=15^0$. (*c*): $\nabla \rho$ plot for NACA0020 profile at $\alpha=20^0$. (*d*): $\nabla \rho$ plot for NACA0012 profile at $\alpha=10^0$. (*e*): $\nabla \rho$ plot for NACA0012 profile at $\alpha=15^0$. (*f*): $\nabla \rho$ plot for NACA0012 profile at $\alpha=20^0$.

Fig-a **Fig-b** **Fig-c**

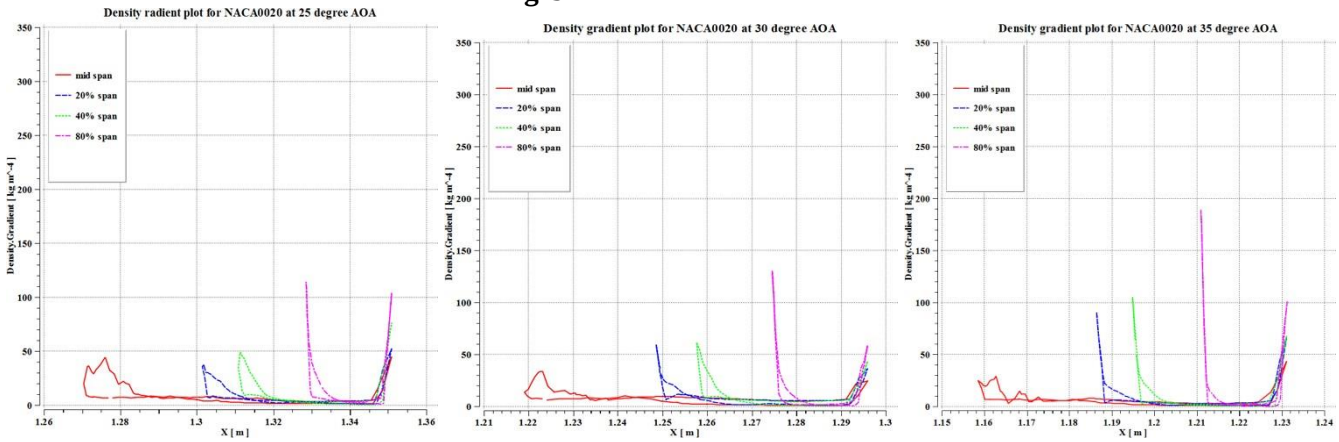

Fig-d **Fig-e** **Fig-f**

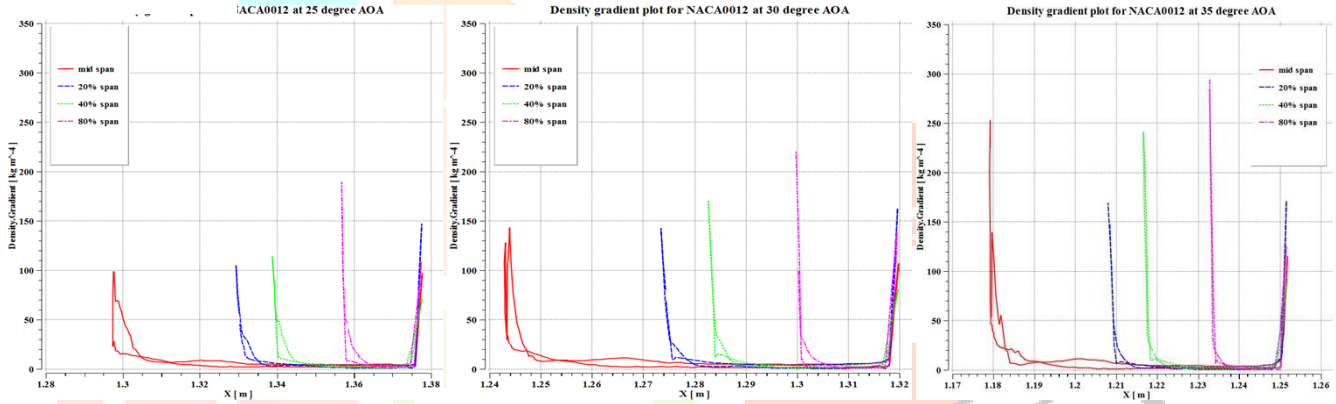

Figure 11 $\nabla \rho$ plot for NACA0020 profile at α=25^0. (*b*): $\nabla \rho$ plot for NACA0020 profile at α=30^0. (*c*): $\nabla \rho$ plot for NACA0020 profile at α=35^0. (*d*): $\nabla \rho$ plot for NACA0012 profile at α=25 ^{0}. (*e*): $\nabla \rho$ plot for NACA0012 profile at α=30^0. (*f*): $\nabla \rho$ plot for NACA0012 profile at α=35^0.

Fig-a **Fig-b** **Fig-c**

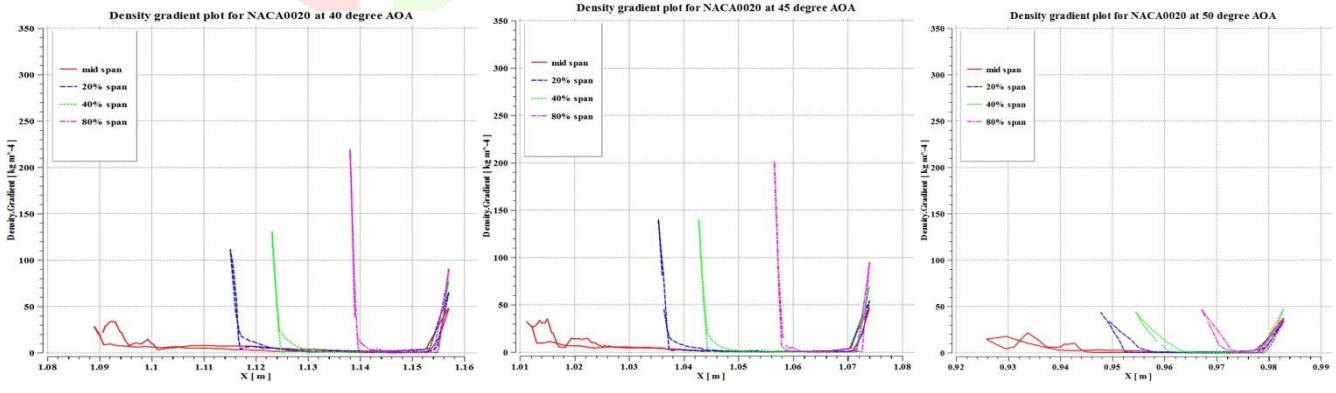

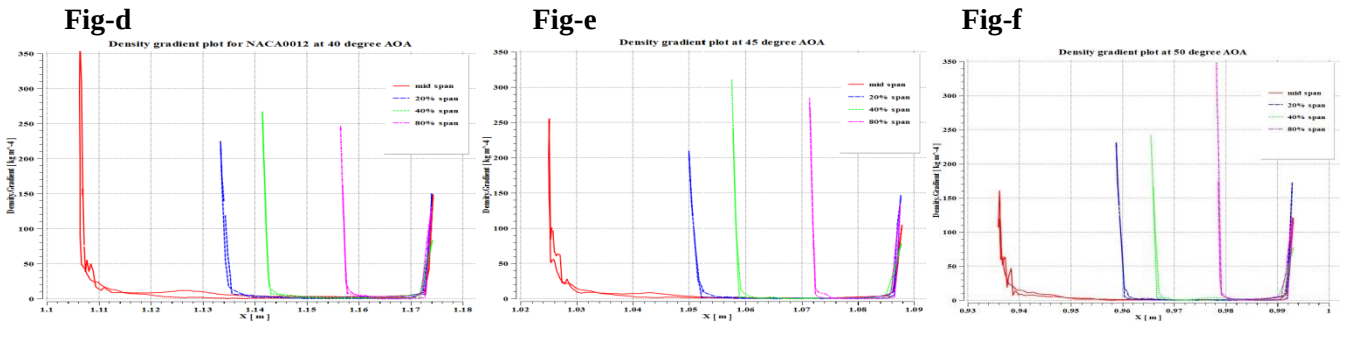

Figure 12 $\nabla \rho$ plot for NACA0020 profile at α=40^0. (*b*): $\nabla \rho$ plot for NACA0020 profile at α=45^0.(*c*): $\nabla \rho$ plot for NACA0020 profile at α=50^0.(*d*): $\nabla \rho$ plot for NACA0012 profile at α=40^0.(*e*): $\nabla \rho$ plot for NACA0012 profile at α=45^0 .(*f*): $\nabla \rho$ plot for NACA0012 profile at α=50^0.

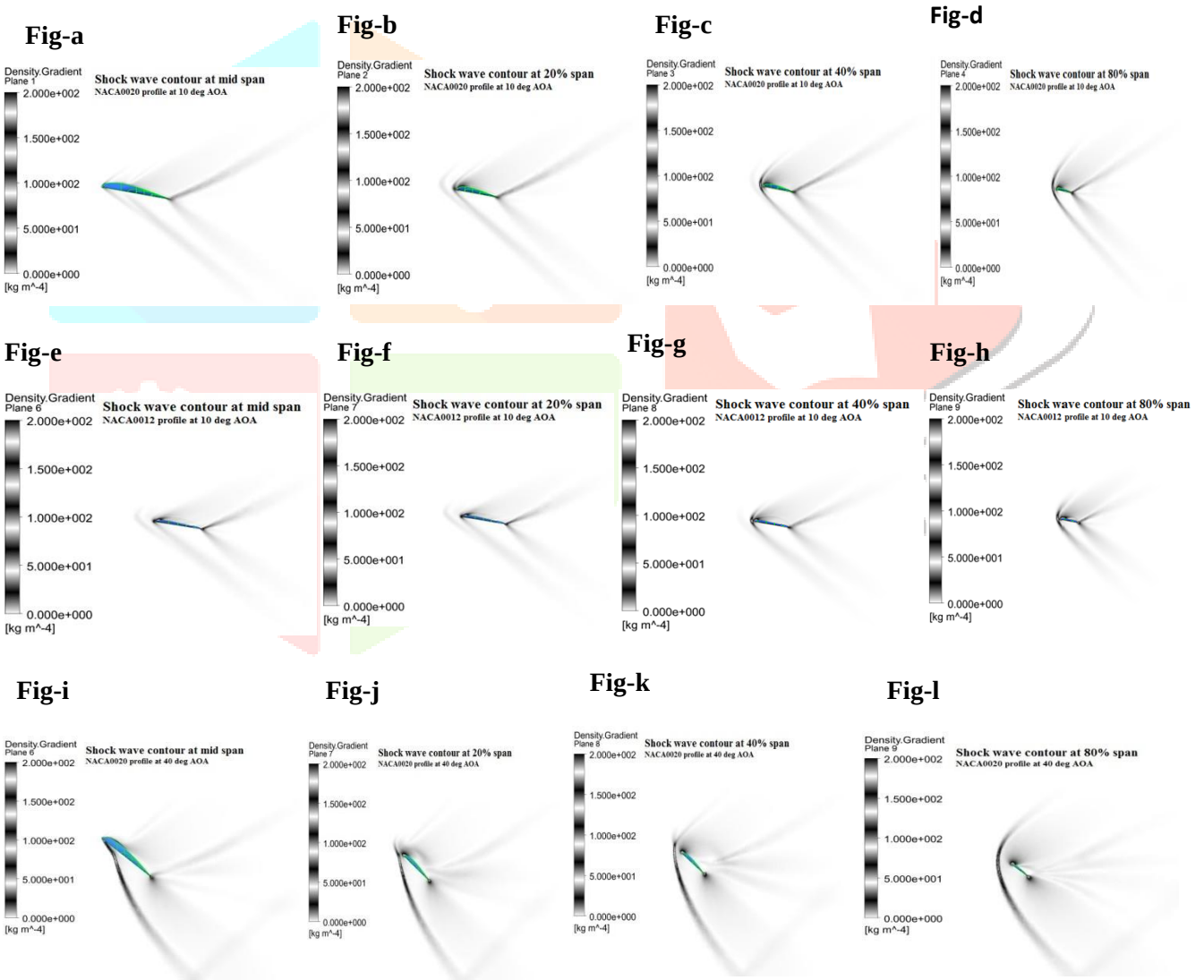

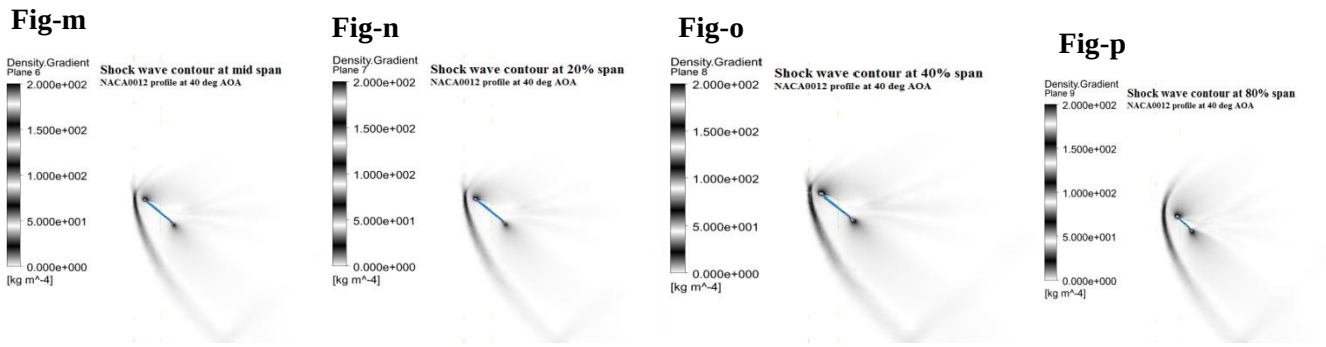

Figure 13 (*a*): Shock wave contour for NACA0020 profile at mid-span and at $\alpha=10^0$. (*b*): Shock wave contour for NACA0020 profile at 20% span and at $\alpha=10^0$. (*c*): Shock wave contour for NACA0020 profile at 40% span and at $\alpha=10^0$. (*d*): Shock wave contour for NACA0020 profile at 80% span and at $\alpha=10^0$. (*e*): Shock wave contour for NACA0012 profile at mid span and at $\alpha=10^0$. (*f*): Shock wave contour for NACA0012 profile at 20% span and at $\alpha=10^0$. (*g*): Shock wave contour for NACA0012 profile at 40% span and at $\alpha=10^0$.(*h*):Shock wave contour for NACA0012 profile at 80% span and at $\alpha=10^0$. (*i*): Shock wave contour for NACA0020 profile at mid span and at $\alpha=40^0$.(*j*): Shock wave contour plot for NACA0020 profile at 20% span and at $\alpha=40^0$.(*k*): Shock wave contour for NACA0020 profile at 40% span and at $\alpha=40^0$.(*l*): Shock wave contour for NACA0020 profile at 80% span and at $\alpha=40^0$.(*m*): Shock wave contour for NACA0012 profile at mid span and at $\alpha=40^0$.(*n*): Shock wave contour for NACA0012 profile at 20% span and at $\alpha=40^0$.(*o*): Shock wave contour for NACA0012 profile at 40% span and at $\alpha=40^0$.(*p*): Shock wave contour for NACA0012 profile at 80% span and at $\alpha=40^0$.

E. COMPARATIVE ANALYSIS OF VORTEX STRUCTURE

Figure.14 shows sectional variations of vorticity over the vehicles at 15%, 50%, and 80% of the mid-chord. Here three α are considered namely $\alpha = 15^0$ (vortices attached to the surface), $\alpha = 30^0$ (before stall), and $\alpha=45^0$ (after stall) respectively. The contour levels are same in all cases, and they are kept in such a way that only strong fluctuations are shown. A strong shockwave cone formed at the nose of re-entry is seen in all lateral planes as an expanding circle. Leading edge vortices generated at the strake are attached to the surface (80% of mid-chord) in both profiles at $\alpha=15^0$ and the wing vortex structure is observed to be more compact for NACA0020 compared to NACA0012. Hence more lift is produced is more for the NACA 0020 profile at $\alpha = 15^0$. The stronger shockwave is observed over the wing surface for NACA0012 profile at $\alpha = 30^0$. The shock wave interacts with the strake and wing vortices create early transition and vortex breakdown over double delta wing for NACA0012 profile. Therefore stalling is achieved earlier for NACA0012 compared to NACA0020. At $\alpha = 45^0$, NACA0012 profile shows compact vortex core region but it is widely distributed for NACA0020 profiles. The bottom surface of the re-vehicle with NACA0012 profile shows higher vortex region. Hence, the C_L is higher for NACA0020 profile. The variation of lift and drag coefficients are discussed in details in the subsequent section.

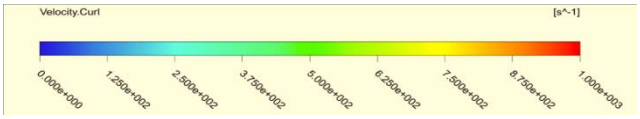

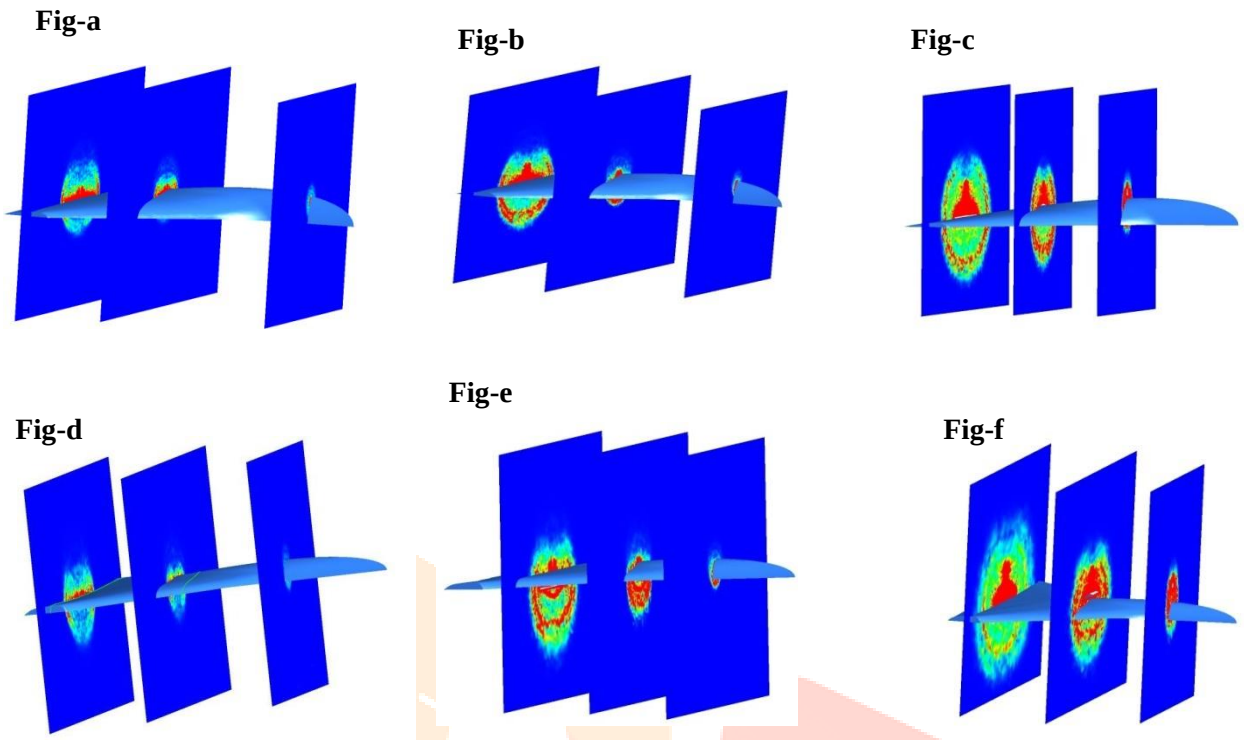

Figure 14 Vortex plot at 15%, 50% and 80% of chord length for NACA 0020 at α=15^0. (*b*): Vortex plot at 15%, 50% and 80% of chord length for NACA0020 at α=30^0.(*c*): Vortex plot at 15%, 50% and 80% of chord length for NACA 0020 at α=45^0.(*d*): Vortex plot at 15%, 50% and 80% of chord length at α=15^0 for NACA0012.(*e*): Vortex plot at 15%, 50% and 80% of chord length at α=30^0 for NACA0012.(*f*): Vortex plot at 15%, 50% and 80% of chord length at α=45^0 for NACA0012.

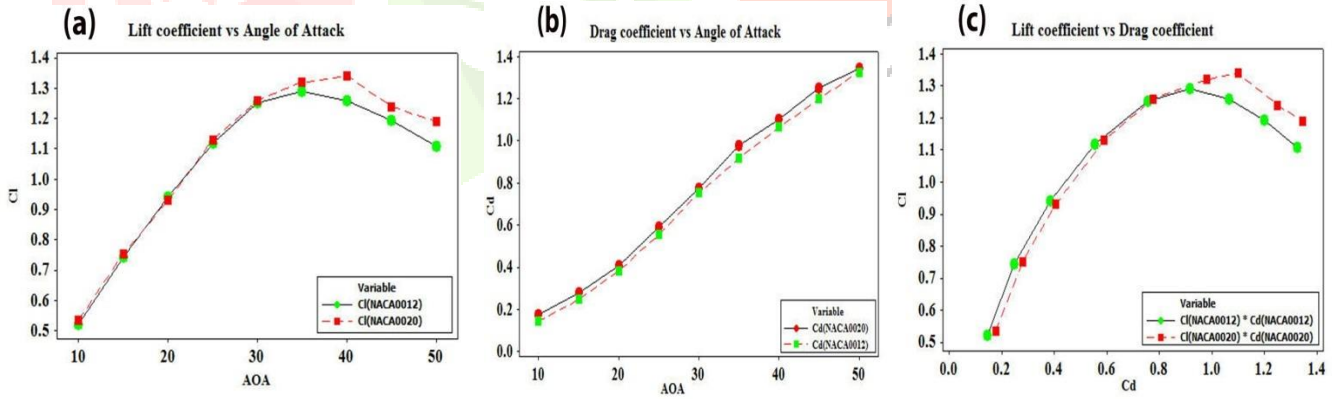

Figure 15 (*a*): Comparative plot for Lift coefficient vs. AOA for NACA0012 and NACA0020 profile. (*b*): Comparative plot for Drag coefficient vs. AOA for NACA0012 and NACA0020 profile. (*c*): Comparative plot of Lift coefficient vs. Drag coefficient.

F. COMPARATIVE ANALYSIS OF FORCE COEFFICIENTS

Lift coefficients, drag coefficients are obtained from the lift and drag convergence monitor. For both NACA0012 profile and NACA0020 profile lift and drag coefficient data for the different angle of attacks are exported to MAT lab and graphs are plotted for the different angle of attacks comparing both the profile as shown in **Fig.15 (a-c).** For NACA0012 profile and NACA0020 profile the drag coefficients, lift coefficients and lift to drag ratios are compared. The maximum value of lift coefficient is observed at 40^0 for NACA0020 profile and for NACA0012 profile it is observed at 35^0. It is found that up to 35^0 the variation of lift coefficient value for both the profiles are minimal (maximum 2.545% at 10^0**)** but beyond this NACA0020 profile is observed to have a higher lift coefficient value. The drag coefficient increases up to 50^0 for both the profiles due to the formation of a shock wave which produces wave drag. It is seen that drag coefficient value is higher for NACA0020 profile for all angle of attacks because of higher thickness. The maximum variation in C_D is observed to be 18.43% at 10^0. Lift coefficient vs. drag coefficient plot showed that for NACA0020 profile up to 40^0 and for NACA0012 profile up to 35^0 both C_L and C_D values are increasing and beyond this C_L is decreasing whereas the C_D value is increasing as shown in Fig.15. The % variation of C_L and C_D for α varying from 10^0 to 50^0 is shown in the **Table-1**.

Table-1

Angle of attack	**10^0**	**15^0**	**20^0**	**25^0**	**30^0**	**35^0**	**40^0**	**45^0**	**50^0**
% variation of C_L	2.545	1.109	1.31	0.974	0.5873	2.2348	6.0074	3.6935	18.475
% variation of C_D	18.43	11.96	5.26	6.11	2.68	6.42	3.19	4.04	2.572

V.CONCLUSION

As coarse mesh solution and fine mesh solution remains invariant, grid dependency study is done for the re-entry vehicle to show the accuracy of meshing for both NACA0012 and NACA0020 profiles. As re-entry vehicle with reflex configuration has not been studied earlier accuracy of simulations are shown through grid dependency test for angle of attack 10^0 to 50^0. The number of elements are considered as 3.6 and 0.3 million respectively. As the finer grid gives more practical result simulations are performed using finer grid. Up to 35^0 both the profiles have shown a minimum variation of lift coefficient. Beyond this NACA0020 profile has shown higher value of C_L compared to NACA0012. At 50^0 angle of attack maximum variation is observed as 18.475%. The optimum angle of attack for the NACA0020 profile is observed at 40^0 but for NACA0012 profile it is found at 35^0. Drag coefficient value is found more in NACA0020 profile due to higher thickness and maximum % variation is observed at lower angle of attacks. 18.43% is observed at $\alpha=10^0$ and 11.96% at $\alpha=15^0$, beyond this maximum variation in drag coefficient is less than 6.42%. Though the maximum variation in drag coefficient between two profiles at 10^0 is observed as 18.43% still the Cd value is 0.1765. Also, the density gradient strength observed for the NACA0020 profile is less compared to NACA0012 profile which shows lower shock strength for NACA0020. Because of higher shock strength the shock wave vortex interaction is happening at earlier values of α for NACA0012. The earlier vortex breakdown is leading to earlier stalling for NACA0012. By observing the CL, CD and shock strength value, NACA0020 profile is observed to be the more suitable profile for re-entry vehicle as it has 40% higher thickness which can accommodate more fuel and electronics components inside the wing. Further experimental studies can be performed for better visualization and quantification of flow physics.

References

[1] Lee, Young-Ki and Kim, Heuy-Dong Vortical flows over a delta wing at high angles of attack. Journal of Mechanical Science and Technology Springer, 2013.

[2] Hebbar, SK and Platzer, MF and Fritzelas, AE. Reynolds number effects on the vortical flow structure generated by a double-delta wing. Experiments in fluids Springer, 2000

[3] Cai, Jinsheng and Pan, Shucheng and Li, Wenfeng and Zhang, Zhengke. Numerical and experimental investigations of a nonslender delta wing with leading-edge vortex flap, Computers & Fluids Elsevier, 2014.

[4] Hoeijmakers, HWM and Vaatstra, W and Verhaagen, NG. Vortex flow over delta and double-delta wings. Journal of aircraft AIAA, 1983.

[5] Reddy, C.S. Modeling effects on the prediction of aerodynamic performance of a double-delta wing. Journal of aircraft AIAA, 1988.

[6] Hsu, C-H and Liu, CH. Navier-Stokes computation of flow around a round-edged double delta wing. AIAA Journal, 1990.

[7] Verhaagen, Nick. Tunnel wall effect on the flow around a 76 ◦ /40 ◦ double-delta wing. 36th AIAA Aerospace Sciences Meeting and Exhibit, 1998.

[8] Sohn, Myong Hwan and Chung, Hyoung Seog. Effects of Strake Planform on the Vortex Flow of a Double Delta Wing. 3rd AIAA Flow Control Conference, 2006

[9] Al-Garni, Ahmad Z and Saeed, Farooq and Al-Garni, Abdullah M. Experimental and numerical investigation of 65 degree Delta and 65/40 degree double-delta wings. Journal of Aircraft American Institute of Aeronautics and Astronautics, 2008

[10] Gonzalez, Hugo A and Erickson, Gary E and McLachlan, Blair G and Bell, James H. Effects of

various fillet shapes on a 76 ◦ /40 ◦ double delta wing from mach 0.18 to 0.7. NAVAL AIR STATION PATUXENT RIVER MD, 2003

[11] Hossain, MD Safayet and Raiyan, Muhammad Ferdous and Akanda, Mohammed Nasir Uddin and Jony, Nahed Hassan. A Comparative flow analysis of NACA 6409 and NACA 4412 aerofoil. International jornal of research in engineering and technology volume 3, 2014

[12] Delery, JM. Shock phenomena in high speed aerodynamics: still a source of major concern. The Aeronautical Journal Cambridge University Press, 1999

[13] Donohoe, SR and Bannink, WJ. Surface reflective visualizations of shock-wave/vortex interactions above a delta wing. AIAA journal, 1997

[14] Kawamura, Takafumi and Mizukaki, Toshiharu. Aerodynamic vibrations caused by a vortex ahead of hemisphere in supersonic flow. 28th International Symposium on Shock Waves Springer, 2012

[15] Sharma, Gaurav and Naimuddin, Mohd and Chopra, Gaurav and Sinha, Jayanta and Sharma, Gagan. Numerical analysis of flow field over compound delta wing at subsonic and supersonic speeds. Aerospace Conference, 2016, IEEE